Complex stationary-phase points in dynamical-tunneling emissions

Soo-Young Lee* and Yunchul Chung
Department of Physics, Pusan National University, Busan 609-735, Korea
(Received 11 April 2011; published 19 October 2011)

In a recent paper [Phys. Rev. A **83**, 023827 (2011)] it has been suggested, based on numerical simulation, that tunneling emission in dielectric microcavities can be explained through a two-step process: first dynamical tunneling to reach the critical line and then interference among tangential wave components refractively escaped from the critical line. Here we investigate again the tunneling-emission mechanism by using a stationary-phase method in a circular microcavity. It is shown that the stationary-phase point becomes complex for a tunneling emission and gives a tunneling-ray picture. The imaginary part of the point determines the distance δ between the tunneling ray and the cavity surface. In addition, we demonstrate numerically that the two-step tunneling process with a proper window function works very well, even in deformed microcavities.

DOI: 10.1103/PhysRevA.84.045805 PACS number(s): 42.55.Sa, 05.45.Mt, 03.65.Xp

One useful property of deformed microcavities is directional emissions of their resonance modes due to broken rotational symmetry. As a cost of the directionality, the quality (Q) factor of the modes generally shows a decreasing behavior as the deformation increases. Both the directionality and the high Q value are sometimes important in various applications such as biosensing, low-threshold microlasers, etc. [1,2]. An optimal combination giving both good directional emission and high Q value can be found in a slightly deformed microcavity in which the degradation of Q value is not appreciable due to the ray dynamical confinement on invariant tori and high-Q modes show only evanescent leakages, i.e., tunneling emission. Understanding the tunneling-emission mechanism is therefore essential to analyze the directionality of the high-Q modes in the slightly deformed microcavity.

In a recent paper [3] it has been suggested that the tunneling emission, characterized by free-space emergence with a finite distance δ from the cavity boundary [4,5], can be explained by a two-step process. The first step is the dynamical tunneling from a torus supporting a high-Q mode to the critical line for total internal reflection in phase space, and the second is the interference between tangential wave components refractively escaped from the critical line. The first dynamical-tunneling process is almost equivalent to a longstanding open problem: a semiclassical understanding of multidimensional tunneling in a nonintegrable system [6,7]. The main difficulty comes from the existence of a natural boundary which prohibits the discovery of a complex tunneling path [8,9]. Apart from the semiclassical description, the two-step process provides a unified picture of the tunneling emission that can be smoothly connected to usual refractive emissions at a larger deformation.

On the other hand, some authors believe that there is a different tunneling emission process, the so-called direct tunneling emission [10]. As for the direct tunneling emission, Creagh and White have developed a theory in an ellipse-shaped microcavity, taking into account the complex tunneling ray dynamics emanating from a complex cavity boundary [11]. It is therefore interesting to find some connection between the two theories on tunneling emission which look quite different.

In this Brief Report we examine the two-step tunneling emission mechanism by using the stationary-phase method in a circular microcavity and show that the stationary-phase points provide a tunneling ray picture similar to the complex ray dynamics [11]. It is also shown that the two-step tunneling emission mechanism works very well even in deformed microcavities if we take a proper window function.

Let us consider tunneling emission in a circular microcavity. According to the two-step process [3], the tunneling emission in a circular microcavity has been described by the interference of tangential wave components brought by the first dynamical tunneling process, as shown schematically in Fig. 1(b), and each tangential wave component has been simulated by a Gaussian beamlike wave as

$$\mathcal{G}(\mathbf{x},\mathbf{s}) = \int d\theta' e^{-(\frac{\theta'-\theta_0}{\Delta\theta})^2} e^{i[k|\mathbf{x}-\mathbf{s}|\cos(\theta'-\theta)+\Phi(\mathbf{s})]}, \qquad (1)$$

where θ and θ_0 are the polar angles of $(\mathbf{x}-\mathbf{s})$ and the tangential direction $\hat{\mathbf{t}}$, respectively [see Fig. 1(a)], and $\Phi(\mathbf{s})$ is the phase of wave function along the boundary. The above equation can be written in the large k limit as

$$\mathcal{G}(\mathbf{x},\mathbf{s}) \simeq \sqrt{\frac{2\pi}{k|\mathbf{x}-\mathbf{s}|}} e^{-(\frac{\theta-\theta_0}{\Delta\theta})^2} e^{i(k|\mathbf{x}-\mathbf{s}|+\Phi(\mathbf{s})+3\pi/4)} \qquad (2)$$

by a stationary-phase method [12] for the θ' integration with a stationary-phase point $\theta' = \theta$. This is a modulated circular wave with a large amplitude in the tangential direction.

Now consider a circular boundary with a radius R and a resonance mode satisfying outgoing-wave boundary conditions. For a high-Q mode showing tunneling emission, the first dynamical-tunneling process to the critical line would give a homogeneous wave function amplitude along the boundary due to the rotational symmetry. Then the wave function outside the cavity would be given by the interference of the tangential wave components coming out from the cavity surface, i.e.,

$$\psi(\mathbf{x}) = \int ds\, \mathcal{G}(\mathbf{x},\mathbf{s}) = R \int d\phi\, \mathcal{G}(\mathbf{x},\mathbf{s}(\phi)), \qquad (3)$$

*pmzsyl@gmail.com

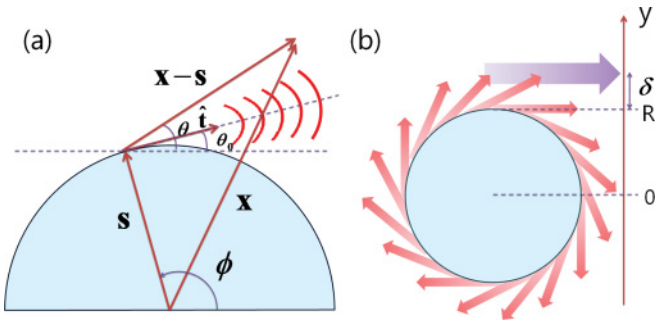

FIG. 1. (Color online) (a) A Gaussian-beam-like wave component propagating in the tangential direction $\hat{\mathbf{t}}$. (b) Schematic diagram for tunneling emission. The tunneling emission (thick arrow) at a distance δ from the boundary surface can be explained by the interference of the tangential wave components (thin arrows) coming out from the boundary surface.

where s is the boundary coordinate, $s = R\phi$, and ϕ the polar angle. Using the modulated circular wave of Eq. (2), the wave function can be rewritten as

$$\psi(\mathbf{x}) = \mathcal{N}\int d\phi\, A(\phi)\, e^{ikf(\phi)}, \tag{4}$$

where

$$A(\phi) = \sqrt{\frac{1}{k\mu(\phi)}}\, e^{-\left(\frac{\nu(\phi)}{\Delta\theta}\right)^2}, \tag{5}$$

$$f(\phi) = \mu(\phi) - nR\sin\chi\phi. \tag{6}$$

Here $\mu(\phi) \equiv |\mathbf{x} - \mathbf{s}(\phi)|$ and $\nu(\phi) \equiv \theta(\phi) - \theta_0(\phi)$, and $\mathcal{N}$ is a constant. For the boundary phase we take $\Phi(\mathbf{s}(\phi)) = -m\phi$, considering a whispering gallery mode with angular quantum number m. The semiclassical relation $\sin\chi = m/nkR$ is used, where χ is the incident angle and n the refractive index.

The stationary-phase method has been widely used to study quantum tunneling appearing in various quantum systems [13–15] and gives an approximate value of the integration, counting up to the second-derivative term in the Taylor expansion of $f(\phi)$ at a stationary-phase point ϕ_0 [12]. The stationary-phase method for the ϕ integration in the large-k limit gives

$$\psi(\mathbf{x}) = \mathcal{N}e^{i\pi/4}A(\phi_0)\, e^{ikf(\phi_0)}\sqrt{\frac{2\pi}{k\frac{d^2f(\phi_0)}{d\phi^2}}}, \tag{7}$$

where ϕ_0 is the stationary-phase point, the solution of the following equation:

$$\frac{df(\phi)}{d\phi} = \frac{d\mu(\phi)}{d\phi} - nR\sin\chi = 0. \tag{8}$$

Since $\mathbf{x} = (x,y)$ and $\mathbf{s} = (R\cos\phi, R\sin\phi)$ [see Fig. 1(a)], $\mu(\phi) = \sqrt{(x - R\cos\phi)^2 + (y - R\sin\phi)^2}$ and its derivative can be expressed as

$$\frac{d\mu}{d\phi} = R(\cos\xi\sin\phi - \sin\xi\cos\phi) = R\sin(\phi - \xi), \tag{9}$$

where $\xi = \cos^{-1}[(x - R\cos\phi)/\mu(\phi)]$. Therefore Eq. (8) with ϕ_0 becomes

$$n\sin\chi = \sin[\phi_0 - \xi(\phi_0)], \tag{10}$$

which is Snell's law, and $(\phi_0 - \xi)$ is nothing but the refraction angle by definition. When the incident angle χ is greater than the critical angle $\chi_c = \sin^{-1}(1/n)$, ϕ_0 should be a complex number to give a sine value greater than 1 in Eq. (10).

In order to get ϕ_0 more explicitly, it would be better to use a different expression of Eq. (8):

$$\frac{x\sin\phi - y\cos\phi}{\mu(\phi)} = n\sin\chi. \tag{11}$$

Using $\phi = \phi_R + i\phi_I$ we arrive at two equations. One is

$$\frac{\beta^2\cosh^2\phi_I - \alpha^2\sinh^2\phi_I}{x^2 + y^2 - 2R\alpha\cosh\phi_I} = (n\sin\chi)^2 \tag{12}$$

and the other is

$$\alpha\cosh\phi_I = n^2R\sin^2\chi, \tag{13}$$

where α and β are functions of x, y, ϕ_R,

$$\alpha(x,y,\phi_R) = x\cos\phi_R + y\sin\phi_R = \mathbf{x}\cdot\hat{\mathbf{r}}_0, \tag{14}$$

$$\beta(x,y,\phi_R) = x\sin\phi_R - y\cos\phi_R = |\mathbf{x}\times\hat{\mathbf{r}}_0|, \tag{15}$$

and $\hat{\mathbf{r}}_0 = (\cos\phi_R, \sin\phi_R)$. From the above two equations we can obtain the complex stationary-phase point ϕ_0 for a given $\mathbf{x} = (x,y)$. Although ϕ_0^* is also a stationary-phase point from Eq. (8), its contribution is exponentially small as giving $\mathrm{Im}[f(\phi_0^*)] > 0$.

The solution of these equations is rather simple. First, the imaginary part of ϕ_0 is given by incident angle χ and independent of $\mathbf{x}$ and ϕ_R, i.e.,

$$\cosh\phi_{0I} = n\sin\chi, \tag{16}$$

and then $\alpha = nR\sin\chi$ from Eq. (13). The real part of ϕ_0, ϕ_{0R} can be then obtained from Eq. (12), i.e.,

$$\beta^2 = |\mathbf{x}|^2\sin^2\zeta = x^2 + y^2 - n^2R^2\sin^2\chi, \tag{17}$$

where ζ is the angle between $\mathbf{x}$ and $\hat{\mathbf{r}}_0$ [see Eq. (15) and Fig. 2]. This means that the ϕ_{0R} is the angle of a right triangle as shown in Fig. 2. The distance between the origin and the right-angle corner is then given as

$$R + \delta = nR\sin\chi, \tag{18}$$

which is the relation expected from the angular momentum conservation [3]. The red arrow of a length $|\mathbf{x}|\sin\zeta$ can be regarded as a tunneling ray.

As an example we consider four tunneling modes, whispering-gallery modes, $M^{WG}(l, m = 60)$, $l = 1,2,3,4$, where l is the radial quantum number. Their wave numbers are $kR \simeq 46.66, 50.80, 54.30, 57.49$, respectively, when $n = \sqrt{2}$ and $R = 1$. They correspond to $\sin\chi = m/nkR \simeq 0.91, 0.84, 0.78, 0.73$ greater than the critical value $\sin\chi_c = 1/n \simeq 0.707$. We consider the y axis at $x = 1.5$ as shown in Fig. 1(b). Figure 3(a) shows ϕ_{0R} as a function of y for the four modes. The constant ϕ_{0I} becomes larger when the mode has higher Q (or larger $\sin\chi$), as shown in Fig. 3(b). In Fig. 3(c) we show, for the mode $M^{WG}(1,60)$, the lines connecting the (x,y) point and the real-space projection of ϕ_0, $(x_0, y_0) = (\mathrm{Re}[R\cos\phi_0], \mathrm{Re}[R\sin\phi_0])$. Each line corresponds to the tunneling ray explained in Fig. 2, and the distance from the cavity surface to the point (x_0, y_0) is $\delta = R(n\sin\chi - 1)$

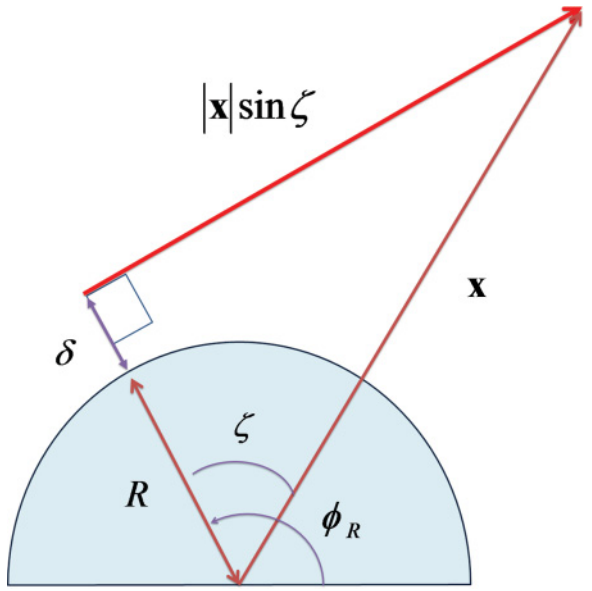

FIG. 2. (Color online) The geometrical description of Eq. (17). The red arrow, starting away from the boundary, corresponds to a tunneling ray.

[see Eq. (18)]. The tunneling rays are consistent with the complex rays in Ref. [11].

To evaluate the wave function of Eq. (7), we used the expressions

$$\frac{d^2 f(\phi_0)}{d\phi^2} = \frac{R}{\mu(\phi_0)}[(x\cos\phi_0 + y\sin\phi_0) - R(n\sin\chi)^2] \tag{19}$$

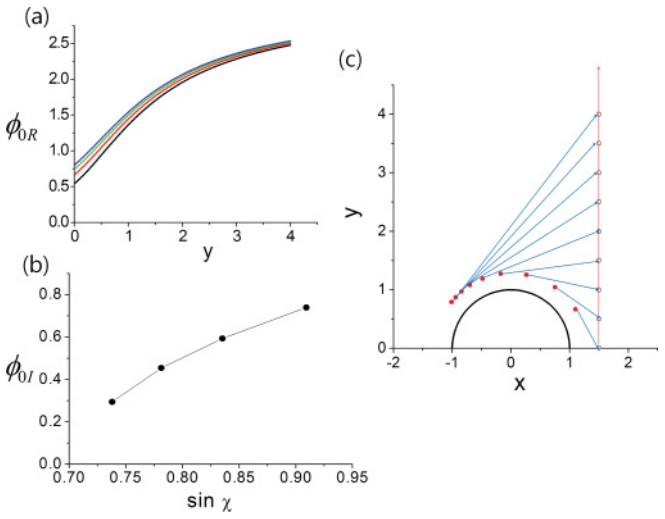

FIG. 3. (Color online) The stationary-phase point ϕ_0. (a) The real part $\phi_{0R}(y)$. The lines correspond to $M^{WG}(l,m=60)$, $l=1,2,3,4$ from the bottom. (b) The constant imaginary part ϕ_{0I}. The dots from right to left correspond to $M^{WG}(l,m=60)$, $l=1,2,3,4$. (c) The real space projection of ϕ_0 (red dots) for given (x,y) (open circles) for $M^{WG}(1,60)$. The connecting lines correspond to the tunneling rays (see Fig. 2).

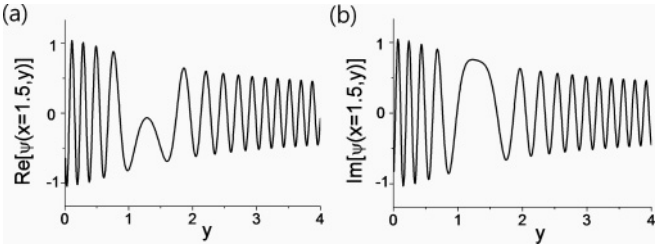

FIG. 4. The wave function $\psi(x=1.5,y)$ [Eq. (7)] for $M^{WG}(1,60)$. (a) The real part. (b) The imaginary part.

and

$$\cos\nu(\phi_0) = \frac{(x\sin\phi_0 - y\cos\phi_0)}{\mu(\phi_0)} = n\sin\chi, \tag{20}$$

which gives $\nu(\phi_0) = i\phi_{0I}$ from the first solution, Eq. (16). This explains why $\Delta\theta$ is insensitive, since the factor $e^{-(\frac{\nu(\phi_0)}{\Delta\theta})^2} = e^{(\frac{\phi_I}{\Delta\theta})^2}$ gives only the overall factor of the wave function due to the constant ϕ_I. Now we calculate the wave function $\psi(x=1,5,y)$ in Eq. (7) by using kR and $\sin\chi$ of the mode $M^{WG}(1,60)$. The real and imaginary parts of $\psi(x=1,5,y)$ are shown in Figs. 4(a) and 4(b), respectively. Their characteristic feature is the slow oscillation near $y \simeq 1.25$, which is related to the tunneling emission with a positive δ as shown below.

In order to probe the tunneling emission directly from the obtained wave function $\psi(x,y)$, we used the emission Husimi functions $H_E(x,y)$ [3] that reveal the intensity of the wave component normally incident on a vertical projection line at x. The emission Husimi functions, $H_E(x=1.5,y)$, are shown in Fig. 5. The peak positions $y_m = R+\delta$ show very good agreement with $nR\sin\chi$ given in Eq. (18), $y_m \simeq 1.286, 1.181, 1.105, 1.044$.

As the microcavity is deformed, the dynamical tunneling rate would not be uniform any longer along the boundary. Then some weighting function varying with s is needed to describe the nonuniform tunneling rate. The width of the function is directly related to the reduction of δ value [3]. The reduction

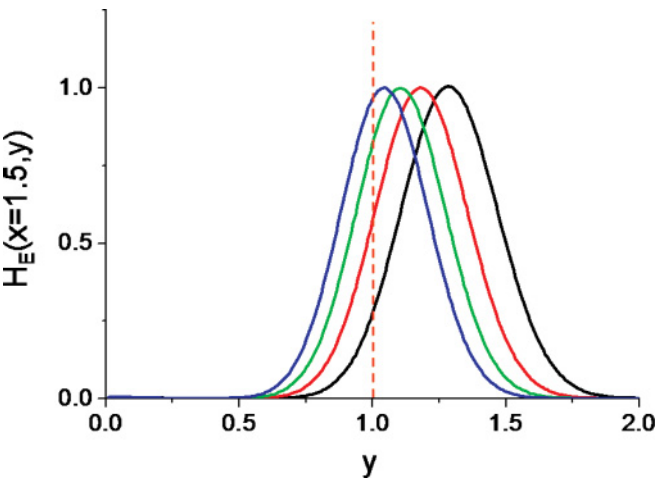

FIG. 5. (Color online) The emission Husimi functions, $H_E(x=1,5,y)$, scaled to give unit peak height. From right to left the lines correspond to $M^{WG}(l,m=60)$, $l=1,2,3,4$. The dashed line indicates the cavity boundary $y=R=1$.

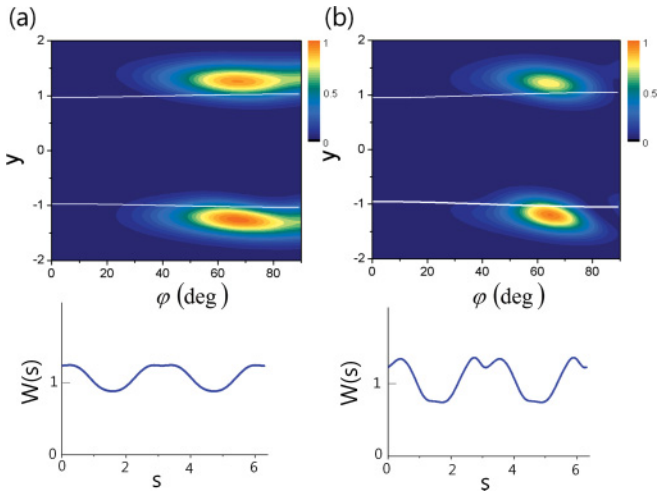

FIG. 6. (Color online) The emission Husimi functions $H_E(\varphi, y)$ and window functions $W(s)$ in a quadrupole deformation. φ is the rotation angle of the projection line [3]. (a) $\varepsilon = 0.03$ case. (b) $\varepsilon = 0.05$ case.

can be easily predicted when we consider the limiting case of weighting or window function $W(s)$. We consider now

$$\psi(\mathbf{x}) = \int ds\, W(s)\mathcal{G}(\mathbf{x},\mathbf{s}). \tag{21}$$

If we take a Gaussian window function $W(\phi) = \frac{1}{(w\pi)^{1/4}} \exp(-\frac{(\phi-\phi_c)^2}{2w})$, giving a maximum weight at $s = s(\phi_c)$. In the small window-width limit, $w \to 0$, the Gaussian function becomes a δ function $\delta(\phi - \phi_c)$. Then the wave function at the limit is given by

$$\psi(\mathbf{x}) = \mathcal{N}\sqrt{\frac{2\pi}{k|\mathbf{x}-\mathbf{s}(\phi_\mathbf{c})|}}\, e^{-(\frac{\theta-\theta_0(\phi_c)}{\Delta\theta})^2} e^{ik|\mathbf{x}-\mathbf{s}(\phi_\mathbf{c})|}. \tag{22}$$

This is a tangential wave component [see Eq. (2)] coming out at $s = s(\phi_c)$, implying zero δ value.

Figure 6 shows emission Husimi functions of the high-Q modes at $\varepsilon = 0.03, 0.05$ in the quadrupole deformation; the modes are traced from $M^{WG}(1,60)$. The wave functions used in the calculation are constructed from the $\mathcal{G}(\mathbf{x},\mathbf{s})$ in Eq. (1) and the $W(s)$ shown in the lower panel in Fig. 6. We take a square root of outgoing Husimi function $H_{\text{out}}(s, p = 1)$ [16] as the $W(s)$, because it corresponds to the amplitude of tangential outgoing waves at the cavity boundary. The boundary phase $\Phi(s)$ has been obtained from the boundary wave function $\psi(s)$. The resulting emission Husimi functions are almost the same as those obtained from real wave functions, Figs. 4(b) and 5(b) of Ref. [3].

In conclusion, we have examined the essential features of tunneling emission in the circular microcavity through the stationary-phase method. The stationary-phase point becomes complex in the tunneling emission case and provides a tunneling ray picture with positive δ, the distance between the tunneling ray and the cavity boundary.

S.Y.L. thanks Creagh for useful discussions. This work was supported by the NRF (Grant No. 2010-0008669) and a KOSEF grant funded by the Korean government (MEST) (Grant No. 2010-0000268).

[1] K. J. Vahala, Nature **424**, 839 (2003).
[2] J. Wiersig and M. Hentschel, Phys. Rev. Lett. **100**, 033901 (2008).
[3] S.-Y. Lee and K. An, Phys. Rev. A **83**, 023827 (2011).
[4] S. C. Creagh, Phys. Rev. Lett. **98**, 153901 (2007).
[5] M. Tomes, K. J. Vahala, and T. Carmon, Opt. Express **17**, 19160 (2009).
[6] A. Shudo and K. S. Ikeda, Phys. Rev. Lett. **74**, 682 (1995).
[7] S. C. Creagh and N. D. Whelan, Phys. Rev. Lett. **77**, 4975 (1996).
[8] J. M. Greene and I. C. Percival, Physica D **3**, 530 (1981); I. C. Percival, *ibid*. **6**, 67 (1982).
[9] S. C. Creagh, in *Tunneling in Complex Systems*, edited by S. Tomsovic (World Scientific, Singapore, 1998).
[10] A. Bäcker, R. Ketzmerick, S. Löck, J. Wiersig, and M. Hentschel, Phys. Rev. A **79**, 063804 (2009).
[11] S. C. Creagh and M. M. White, J. Phys. A: Math. Theor. **43**, 465102 (2010).
[12] J. D. Jackson, *Classical Electrodynamics* (John Wiley & Sons, 1975).
[13] E. O. Kane, J. Appl. Phys. **32**, 83 (1961).
[14] M. Wilkinson, Physica D **21**, 341 (1986).
[15] H. G. Winful, Phys. Rev. Lett. **91**, 260401 (2003).
[16] M. Hentschel, H. Schomerus, and R. Schubert, Europhys. Lett. **62**, 636 (2003).